A 2D FOURIER APPROACH TO DEFORMABLE MODEL SEGMENTATION OF 3D MEDICAL IMAGES

Eric Berg[1], *Mohamed Mahfouz*[2, 3], *Christian Debrunner*[1], *William Hoff*[1]
[1] Colorado School of Mines, Golden, Colorado, [2] University of Tennessee, Knoxville, Tennessee
[3] Oak Ridge National Laboratories, Oak Ridge, Tennessee

ABSTRACT

Anatomical shapes present a unique problem in terms of accurate representation and medical image segmentation. Three-dimensional (3D) statistical shape models have been extensively researched as a means of autonomously segmenting and representing models. We present a method based on a principal component analysis of a stack of 2D contours represented as Fourier descriptors (FDs). A training set for the shape model is generated directly from the FDs of the perimeters of the segmented regions on each image after a transformation into a canonical coordinate frame. We apply our shape model to the segmentation of CT and MRI images of the distal femur via an iterative method based on active contours. Results of the application of our method demonstrate its ability to accurately capture shape variations and guide segmentation.

1. INTRODUCTION

Current methods in three-dimensional image segmentation typically employ statistical shape models, first developed by Cootes and Taylor [1] as a means to incorporate a priori shape information. Principal component analysis highlights the primary modes of variation among instances of the shape, allowing for a potential reduction in the dimension of the shape space.

A critical requirement of shape models is to find correspondences among instances of the shape to be modeled. Shape models can be built from 2D contours, eg. [1] and 3D surfaces, eg. [2], where corresponding control points, or landmarks, are manually identified on each shape instance. Manual selection of control points can be tedious and often unreliable due to the subjectivity of point selection [3].

Our 3D shape model is constructed as a stack of 2D contours, each of which is converted to a Fourier descriptor (FD) representation after the stack of contours is transformed into a canonical coordinate frame. Unlike some existing methods, we form a model vector with the FDs from all of the contours in a given model, thus allowing the identification of inter-slice relationships in addition to the in-slice relationships. Our segmentation algorithm includes an iterative process of contour adjustment via a traditional active contours technique [4], followed by a projection into the shape space defined by the principal components.

We tested our method on 19 available image sets of the distal femur with mixed MRI and CT datasets. Our currently available datasets of the distal femur include both left and right femurs, so we mirrored the left femur across the midsagittal plane as was done in [5, 6], creating additional samples of the right femur.

The automated model-based segmentation yields a stack of 2D contours, which are then combined into a 3D surface model. Results of the automated segmentation are compared to a manual segmentation of the same datasets through a slice-by-slice analysis.

2. APPROACH

Our method consists of two main steps – constructing a statistical shape model from a set of training shapes, and autonomous segmentation of similar shapes in 3D medical images, guided by the statistical shape model. The statistical shape model represents the average of the training shapes along with the primary modes of variation among the shapes. Model-based segmentation produces a new model whose shape must conform to the training shapes used to form the model.

2.1. Image preprocessing

Each 3D image volume to be used as a training set is manually segmented to extract the distal section of the femur. The binary (black and white) images resulting from the segmentation are rigidly registered to a coordinate system as shown in Figure 1. The z-axis passes approximately through the center of the condyles and through the center of the shaft approximately 120mm above the condyles. The x-axis coincides with a line drawn between the center of the medial and lateral condyles and intersects the distal end of the z-axis. The y-axis is positive in the posterior direction.

This work was funded by Depuy Orthopaedics, Inc., a division of Johnson & Johnson, Warsaw, Indiana.

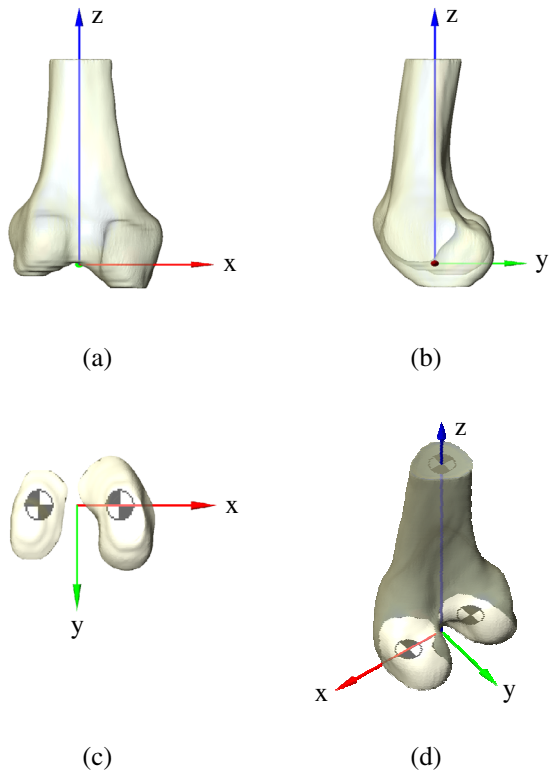

Fig. 1. Coordinate frame definition showing (a) coronal view (b) sagittal view (c) axial view, and (d) isometric view.

2.2. Fourier descriptors

Each binary image resulting from the segmentation contains at least one region representing the bone cross-section; in the case of images intersecting the condyles, two regions may be present. The regions on each slice can be reduced to closed contours, allowing for a FD representation to be computed. FDs were originally developed by [7] for use in shape discrimination and identification as in [8]. Our method uses FDs to normalize contours of unequal length and shape and to reduce the amount of data required to store each model.

Each contour is defined by a set of N perimeter pixels (Figure 2), whose indices, after multiplication by the pixel size in millimeters, represent the x and y coordinates. We can ignore the pixel size for the purpose of computing the FDs since the preprocessing steps ensure that all images have the same pixel size. This allows us to simply use the pixel indices, which are all integer values.

The pixel locations are represented as a vector of the form,

$$s = (s_1 \;\; s_2 \;\; \ldots \;\; s_N)^T, \qquad (1)$$

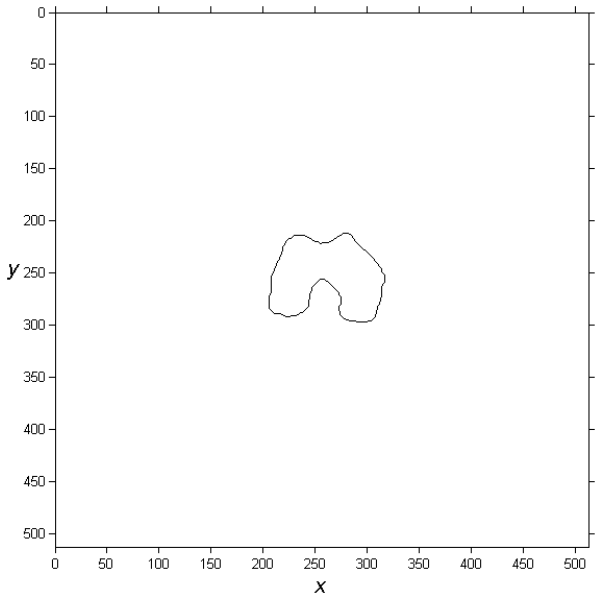

Fig. 2. Plot showing the coordinate system used to define the pixel locations (512 x 512 image).

where $s_i = x_i + jy_i$ and j is $\sqrt{-1}$. The 2D FDs are computed via the discrete Fourier transform (DFT) as follows:

$$a(k) = \frac{1}{N}\sum_{q=0}^{N-1} s(q)\exp(\tfrac{-j2\pi qk}{N}), \qquad (2)$$

where the values of k are the indices *0,1,…,N-1*.

The symmetry of the Fourier transform allows a reduction in the number of coefficients required to accurately reconstruct the original contour. The highest magnitude Fourier coefficients occur in the low frequency spectrum and we can take advantage of this symmetry by removing the high frequency coefficients. We found through experiment that 32 coefficients sufficiently described the shape of all femoral cross-sections. To reconstruct a contour with N' points from this reduced form, the FD vector a' must be constructed as follows,

$$a' = (a_1 \;\; \ldots \; a_{16} \;\; 0 \;\; \ldots \;\; 0 \;\; a_{N'-15} \;\; \ldots \;\; a_{N'})^T, \qquad (3)$$

where the number of zeros to be inserted is $N' - 32$, assuming $N > 32$. The vector is padded with zeros to create a vector of length N', while maintaining the exact shape of the contour as described by the 32 coefficients. The effect of the additional terms in a' is to increase the number of points to be reconstructed from the FDs. The reconstruction of the contour points is achieved through the inverse Fourier transform,

$$s(q) = N'\sum_{k=0}^{N'-1} a'(k)\exp(\tfrac{j2\pi kq}{N'}). \qquad (4)$$

After rounding the reconstructed coordinates to the nearest pixel, it is important to note that if $N' > N$, $s(q)$ will occasionally have repeated values representing the same pixel location. If the goal is to reconstruct images from the FDs, then this is not a problem; however, if the points are to be used in an algorithm such as iterative closest point (ICP) matching, the duplicated points should be removed to avoid improper point weighting.

2.3. Shape model representation and construction

Each femur model is composed of M contour slices parallel to the axial plane (Figure 3), where the z-axis is normal to the axial plane. Each of the M contours is described by Q FDs, which are complex pairs as prescribed by (1) and (2). A contour is represented by a single vector formed by concatenating the real and imaginary parts of the Q FD coefficients that represent it. The model vector m is then formed by concatenating the M contour vectors to form a vector of length $n = 2QM$. The multiple of 2 is due to the real and imaginary part of each FD.

For a set of T models, the n x 1 mean vector, $\overline{m}$ is calculated by,

$$\overline{m} = \frac{1}{T}\sum_{i=1}^{T} m_i \,. \tag{5}$$

The modes of variation among the bone models can be determined using principal component analysis (PCA). First, we must subtract the mean vector, $\overline{m}$, from each $\overline{m}_i$, forming a matrix whose columns are the deviation vectors,

$$dm_i = m_i - \overline{m} \,. \tag{6}$$

The PCA is performed as an eigendecomposition of the T x T deviation matrix $dm\, dm^T$ as follows,

$$\frac{1}{T-1} dm\, dm^T p_k = \lambda_k p_k \,, \tag{7}$$

where p_k is the k^{th} orthonormal eigenvector of $dm\, dm^T$ and λ_k is the eigenvalue corresponding to p_k. Arranging the eigenvalues in descending order and reordering the eigenvectors accordingly, we can determine the principal components, or the eigenvectors that account for the most significant variance.

Any shape instance in the training set can be represented by the mean model and a linear combination of the eigenvectors [9]. Typically, we can accurately represent a model with $t < T$ modes, which capture the significant variances. The modes corresponding to the largest t eigenvalues, or the principal components, are used since they describe the greatest variance. As Cootes et al. [10] and Hutton et al. [11] point out, we can assume that the principal components representing 98% of the variance are sufficient to capture the variability in the model, while the remaining 2% is considered noise. A model can then be approximated as,

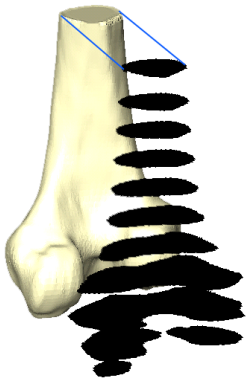

Fig. 3. Model of the distal femur demonstrating the slice structure. Note that the slices shown are a select few of the total number of slices.

$$m = \overline{m} + \sum_{i=1}^{t} \alpha_i p_i \,, \tag{8}$$

where α_i is the coefficient multiplying the i^{th} principal component. This representation allows us to store the mean model vector and the vectors corresponding to the first t PCs.

2.4. 3D image segmentation

A 3D image volume that is not included in the training set can be segmented by iteratively deforming the FD model until the deformed model closely matches the image set. The contours, whose FDs describe the model, are adjusted by active contours [4], where the external driving force is the gradient on each image. The FDs of the adjusted contours are projected onto the principal component space in equation 8. This projection provides a constraint on possible shapes to prevent segmentations that are inconsistent with the training shapes. The alternating process of active contour deformation and shape space projection continues until the following convergence function reaches some empirical threshold,

$$\Delta = \sum_{i=1}^{t} \left(\alpha_{ni} - \alpha_{(n-1)i}\right)^2 \qquad \text{for n > 1,} \tag{9}$$

where Δ represents the change in the model parameters from one iteration to the next. When this squared sum is less than the specified threshold, the model is assumed to have converged on a solution.

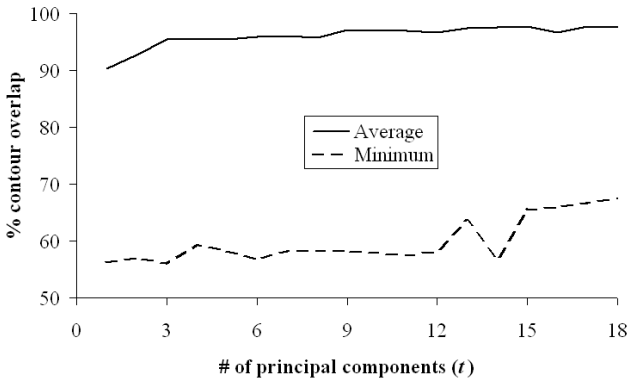

Fig. 4. Average and minimum percentage of model segmented perimeters within two pixels of the manually segmented perimeters for values of *t* ranging from 1 to 18.

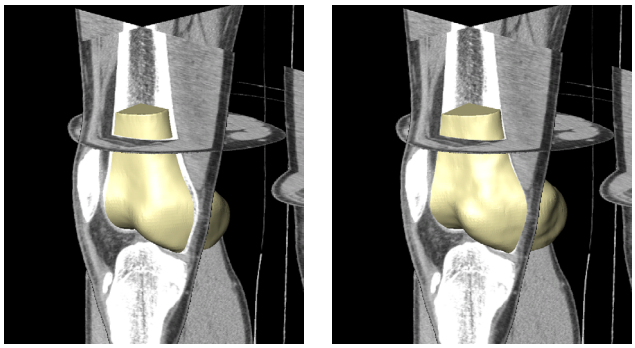

Fig. 5. Initial mean model (left) and final, autonomously segmented model (right).

3. RESULTS AND CONCLUSION

A test of the method was done using a leave-one-out approach, see eg. [12], where all but one of the 19 available image volumes are used as training shapes, while the remaining image volume is segmented using the shape model. The test is performed for all 19 image volumes; once for each image set, and we compare the autonomous model-based segmentation results to the manual segmentation of that image volume. Additionally, the results of tests performed with a varying number of principal components (t = 1, 2 … 18) are compared, demonstrating that more principal components result in a better segmentation.

The quality of the segmentation is measured by the percentage of each perimeter of the automatically segmented regions that falls within two pixels (1.5 mm) of the perimeter of the corresponding manually segmented regions. This percentage is averaged over the M slices in the model (Figure 4).

Figure 5 shows the starting model (mean) for a selected training set and the final model created from the autonomous segmentation of the left out image volume. Also shown are some images from the autonomously segmented image set interpolated in the axial, sagittal and coronal planes.

Our shape modeling and segmentation methods have produced promising results for the distal femur. The methods presented in this paper are readily extended to other bones.

4. REFERENCES

[1] T. Cootes and C. Taylor, "Active shape models—'Smart snakes'," Proc. British Mach. Vision Conf., pp. 266-275, 1992.

[2] S. Benameur, M. Mignotte, S. Parent, H. Labelle, W. Skalli, and J. de Guise, "3D Biplanar Reconstruction of Scoliotic Vertebrae Using Statistical Models", 2001 IEEE Computer Society Conference on Computer Vision and Pattern Recognition, pp. II-577-582, 8-14, Dec 2001.

[3] R. Davies , C. Twining, T. Cootes, J. Waterton, and C. Taylor, "A Minimum Description Length Approach to Statistical Shape Modeling," IEEE Transactions on Medical Imaging, Vol. 21, No. 5, pp. 525-537, May 2002.

[4] M. Kass, A. Witkin, and D. Terzopoulos, "Snakes: Active contour models," Int. J. Comput. Vis., vol. 1, pp. 321–331, 1987.

[5] C. Taylor, T. Cootes, A. Hill, and J. Haslam, "Medical Image Segmentation Using Active Shape Models," Proc. Medical Imaging Workshop, Brusseles, Belgium, pp. 121-143, 1995.

[6] M. Kaus, V. Pekar, C. Lorenz, R. Truyen, S. Lobregt, and J. Weese, "Automated 3-D PDM Construction from Segmented Images Using Deformable Models," IEEE Transactions on Medical Imaging, Vol. 22, No. 8, pp. 1005-1013, Aug 2003.

[7] C. Zahn and R. Roskies, "Fourier Descriptors for Plane Closed Curves," IEEE Transactions on Computers, Vol. 21, No. 3, pp. 269-281, Mar 1972.

[8] E. Persoon and K. Fu, "Shape Discrimination Using Fourier Descriptors," IEEE Trans. on Sys.,Man, and Cyber., vol. SMC-7, no. 3, pp. 629-639, Mar 1977.

[9] T. Cootes, A. Hill, C. Taylor, and J. Haslam, "The Use of Active Shape Models for Locating Structures in Medical Images," Image and Vision Computing, vol. 12, no. 6, pp. 355-365, Jul 1994.

[10] T. Cootes, G. Edwards, and C. Taylor, "Active appearance models," in Proc. Eur. Conf. Computer Vision, vol. 2, H. Burkhardt and B. Neumann, Eds, pp. 484–498, 1998.

[11] T. Hutton , B. Buxton, P. Hammond, and H. Potts, "Estimating Average Growth trajectories in Shape-Space Using Kernel Smoothing," IEEE Transactions on Medical Imaging, Vol. 22, No. 6, pp. 747-753, Jun 2003.

[12] A. Kelemen, G. Székely, and G. Gerig, "Elastic Model-Based Segmentation of 3-D Neuroradiological Data Sets," IEEE Transactions on Medical Imaging, Vol. 18, No. 10, pp. 828-839, Oct 1999.